Atmospheric Environment 180 (2018) 184–191

Contents lists available at ScienceDirect

Atmospheric Environment

journal homepage: www.elsevier.com/locate/atmosenv

Enhanced light absorption due to the mixing state of black carbon in fresh biomass burning emissions

Qiyuan Wang[a,*], Junji Cao[a,b,**], Yongming Han[a,c], Jie Tian[d], Yue Zhang[d], Siwatt Pongpiachan[e], Yonggang Zhang[a], Li Li[a], Xinyi Niu[c], Zhenxing Shen[d], Zhuzi Zhao[a], Danai Tipmanee[f], Suratta Bunsomboonsakul[e], Yang Chen[g], Jian Sun[d]

[a] Key Laboratory of Aerosol Chemistry and Physics, State Key Laboratory of Loess and Quaternary Geology, Institute of Earth Environment, Chinese Academy of Sciences, Xi'an, 710061, China
[b] Institute of Global Environmental Change, Xi'an Jiaotong University, Xi'an, 710049, China
[c] School of Human Settlements and Civil Engineering, Xi'an Jiaotong University, Xi'an, 710049, China
[d] Department of Environmental Science and Engineering, School of Energy and Power Engineering, Xi'an Jiaotong University, Xi'an, 710049, China
[e] School of Social & Environmental Development, National Institute of Development Administration (NIDA), Bangkok, 10240, Thailand
[f] Faculty of Technology and Environment, Prince of Songkla University, Phuket Campus, Kathu, Phuket, 83120, Thailand
[g] Chongqing Institute of Green and Intelligent Technology, Chinese Academy of Sciences, Chongqing, 400714, China

GRAPHICAL ABSTRACT

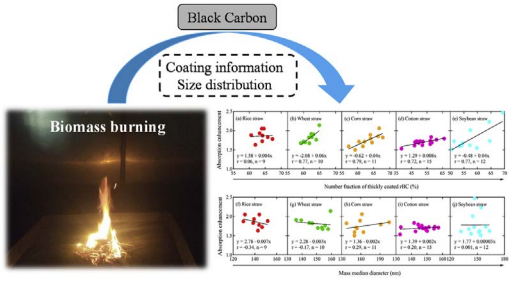

ARTICLE INFO

Keywords:
Black carbon
Mixing state
Size distribution
Light absorption
Biomass burning

ABSTRACT

A lack of information on the radiative effects of refractory black carbon (rBC) emitted from biomass burning is a significant gap in our understanding of climate change. A custom-made combustion chamber was used to simulate the open burning of crop residues and investigate the impacts of rBC size and mixing state on the particles' optical properties. Average rBC mass median diameters ranged from 141 to 162 nm for the rBC produced from different types of crop residues. The number fraction of thickly-coated rBC varied from 53 to 64%, suggesting that a majority of the freshly emitted rBC were internally mixed. By comparing the result of observed mass absorption cross-section to that calculated with Mie theory, large light absorption enhancement factors (1.7–1.9) were found for coated particles relative to uncoated cores. These effects were strongly positively correlated with the percentage of coated particles but independent of rBC core size. We suggest that rBC from open biomass burning may have strong impact on air pollution and radiative forcing immediately after their production.

* Corresponding author.
** Corresponding author. Key Laboratory of Aerosol Chemistry and Physics, State Key Laboratory of Loess and Quaternary Geology, Institute of Earth Environment, Chinese Academy of Sciences, Xi'an, 710061, China.
E-mail addresses: wangqy@ieecas.cn (Q. Wang), cao@loess.llqg.ac.cn (J. Cao).

https://doi.org/10.1016/j.atmosenv.2018.02.049
Received 29 December 2017; Received in revised form 21 February 2018; Accepted 26 February 2018
Available online 01 March 2018
1352-2310/ © 2018 Elsevier Ltd. All rights reserved.

1. Introduction

Black carbon (BC) is produced during the incomplete combustion of carbon-containing materials, and it is the dominant light-absorbing form of atmospheric particulate matter for visible and infrared wavelengths of light (Bond et al., 2013). Light absorption by anthropogenic BC particles can perturb the Earth's radiative balance and in so doing cause warming aloft and surface dimming on both regional and global scales (Ramanathan and Carmichael, 2008; Booth and Bellouin, 2015). Climate modeling studies indicate that BC is the second largest contributor to current global warming after carbon dioxide (CO_2) (Jacobson, 2001; Bond et al., 2013). In addition, BC plays an important role in haze pollution through its impacts on the aerosol-planetary boundary layer (Ding et al., 2016). Further, BC is associated with adverse impacts on human health and crop yields (Tollefsen et al., 2009; Li et al., 2016), and it also has been linked to reductions in precipitation and negative influences on terrestrial and aquatic ecosystems (Forbes et al., 2006; Hodnebrog et al., 2016).

Estimates from modeling studies indicate that the direct radiative forcing caused by BC is about $+0.71\ W\ m^{-2}$, but the uncertainty of the estimates is large, ~90%, ranging from $+0.08$ to $+1.27\ W\ m^{-2}$ (Bond et al., 2013). One of the difficulties in making reliable estimates of BC radiative effects is that the calculations are sensitive to whether the particles are treated as internally- or externally-mixed with non-BC materials (Bauer et al., 2010). Furthermore, there also are still uncertainties concerning the effects of BC mixing state on light absorption. Both laboratory studies and field measurements have shown that particles' light absorption can be enhanced by the internally-mixed BC. For example, Liu et al. (2015) demonstrated clearly that coatings can substantially enhance light absorption, with the magnitude strongly depending on extent of the BC coatings and their sources. Wang et al. (2014a) reported an absorption enhancement of 1.8 in a polluted urban city of China due to the large percentage of coated BC particles. Peng et al. (2016) found an absorption amplification factor of 2.4 for BC particles after they aged several hours. In contrast, however, Cappa et al. (2012) observed a small BC absorption enhancement of only 6% at two sites in California, and the effect increased weakly with photochemical aging. Lan et al. (2013) similarly found that coated BC particles only amplified light absorption by ~7% in an urban atmosphere of South China. These discrepancies may be attributed to several factors, such as particle's size, shape, and coatings as well as the emission sources. Our understanding of how the BC mixing state affects the particles' light absorption is still limited.

Biomass burning is one of the largest sources for BC in the global atmosphere (Bond et al., 2013). In China, open biomass burning is an especially important contributor to BC and estimated to be 137 Gg in 2013 (Qiu et al., 2016). Of the biomass sources, the burning of crop residues (e.g., rice, wheat, and corn) has its most significant impact on BC emissions during the summer/autumn harvest seasons. The traditional method of “slash and burn” agricultural is often used to clear fields of leftover plant residues and return nutrients to the soil. Although the Chinese government has taken measures to prohibit the open burning of agricultural crop residues, local enforcement of the regulations is still uneven. According to the agricultural fire map from Zha et al. (2013), the numbers of total agricultural fire sites in China were 5514 in 2009 and 4225 in 2010, and > 80% of them were distributed in the agricultural regions. Moreover, recent studies have shown that crop field burning activities not only led to local air pollution but also had effects on regional air quality through the transport and dispersal of pollutants (Long et al., 2016).

Studies on BC emissions from open burning of crop residues in China have been presented in previous publications (Chen et al., 2017, and references therein), but limited investigations have specifically focused on the effects of the BC size and mixing state on particles' optical properties. In this study, a custom-made combustion chamber was used to simulate the open burning of several representative types of crop residues. We demonstrate substantial light absorption enhancement of refractory BC (rBC) in fresh biomass-burning emissions relative to uncoated particle cores. Through detailed physicochemical analyses, we show that the absorption enhancement is strongly related to the amounts of coatings on the rBC particles. The results contribute to our understanding of the optical properties of rBC particles produced through biomass burning.

2. Experimental methods

2.1. Combustion chamber experiment

Test burns were conducted in a custom-made combustion chamber at the Institute of Earth Environment, Chinese Academy of Sciences (IEECAS) to simulate the open burning of crop residues. The combustion chamber is a $\sim 8\ m^3$ cavity container with a length, width, and height of 1.8, 1.8, and 2.2 m, respectively. The chamber has 3 mm thick passivated aluminum walls to withstand high combustion temperatures inside the chamber. The combustion chamber is equipped with a thermocouple, a thermoanemometer, and an air purification system. A dilution sampler (Model 18, Baldwin Environmental Inc., Reno, NV, USA) was installed downstream of the chamber to dilute the smoke before sampling. A schematic of the instrumental setups of the experiments is shown in Fig. 1. Tian et al. (2015) provided a detailed description of the structure and evaluation of this combustion chamber.

Samples of rice, wheat, corn, cotton, and soybean straw and stalks were collected from seven major Chinese crop producing provinces (e.g., Shandong, Shaanxi, Hunan, Henan, Hebei, Jiangxi, and Anhui), which accounted for ~40% of total mass of those crops in China in 2015 (China Statistical Yearbook, 2016). Meanwhile, Ni et al. (2015) have pointed out that there are no significant differences in $PM_{2.5}$ chemical source profiles for the same crop residues from different regions. The samples were stored at a stable temperature of ~20 °C and relative humidity of 35–45% for at least one month before burning. Aliquots of ~52 g were weighed, and the samples were burned on a platform inside the combustion chamber for ~5–10 min. The smoke emitted from each test burn was first diluted with the dilution sampler and then sampled by several on-line instruments downstream. The dilution ratio was ~20–25 for most burning cases. A total of 57 tests were conducted as follows: 9 for rice straw, 10 for wheat straw, 11 for corn stalks, 15 for cotton stalks, and 12 for soybean stalks. Detailed information on each test burn is summarized in Table 1.

2.2. Quantification of rBC mass, size and mixing state

The mass, size, and mixing state of rBC particles were determined with a single-particle soot photometer (SP2, Droplet Measurement Technology, Boulder, CO, USA), which uses a laser-induced incandescence for the measurements (Schwarz et al., 2006; Gao et al., 2007). An rBC particle that enters the instrument is heated by an intracavity Nd: YAG laser (λ = 1064 nm) to its vaporization temperature, and that causes the emission of thermal radiation, which is measured by two types of optical detectors. The peak incandescence signal is proportional to the rBC mass, and it is not affected by the particle morphology or mixing state (Slowik et al., 2007). In this study, the peak intensity of the incandescence signal was converted to rBC mass using a standard fullerene soot sample (Lot F12S011, Alfa Aesar, Inc., Ward Hill, MA, USA). An atomizer (Model 9302, TSI Inc., Shoreview, MN, USA) was used to generate BC particles from the fullerene soot. After the particles passed through a diffusion silica-gel dryer, they were size-selected with a differential mobility analyzer (Model 3080, TSI Inc.) before the instrumental analysis. The uncertainty of the SP2 measurements is ~20%. Detailed descriptions of the SP2 calibration procedures can be found in our previous publications (Wang et al., 2014a, 2014b).

The mass-equivalent diameters of rBC cores were calculated from the measured rBC masses by assuming the rBC particles were solid

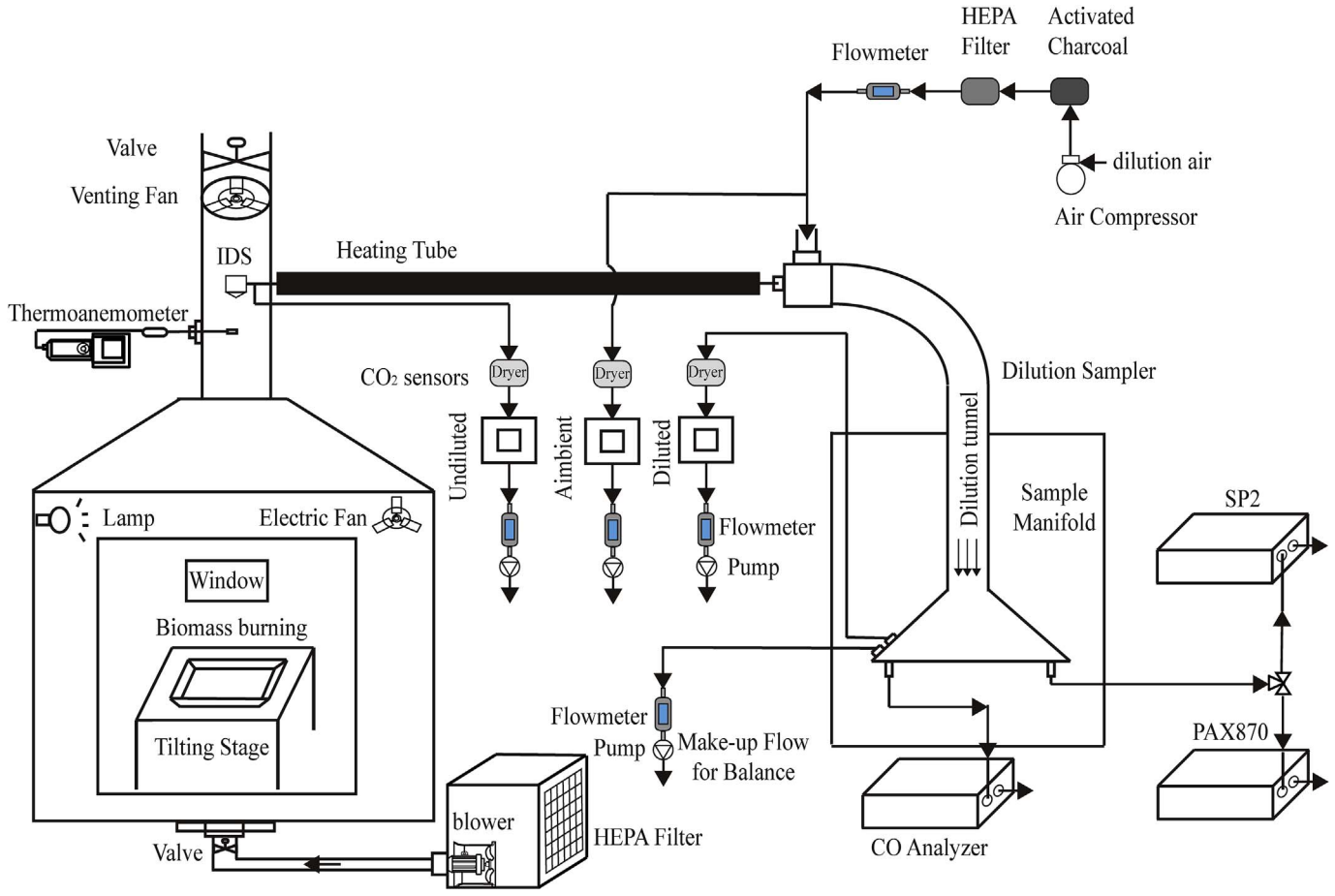

Fig. 1. Schematic of the instrumental setups of the experiments.

spheres with a density of 1.8 g cm^{-3} (Bond and Bergstrom, 2006), and the values ranged from ~70 to 700 nm (see Fig. 2). It is important to note that the rBC core sizes measured in this way do not include the contributions of non-rBC materials to the particle diameter because those materials are vaporized as described above. The rBC mass fraction outside the lower and upper particle size limits for the SP2 (~10%) was estimated by fitting a log-normal distribution to the measured rBC mass-size distribution (Wang et al., 2016a).

The rBC mixing state was characterized by the lag-time between the peaks of incandescence and scattering signals. The lag-time occurs because coatings have to be removed from the rBC core before incandescent temperatures of the cores are reached. Fig. 3 shows that the lag-times displayed a bimodal distribution with ~2 μs separating two distinct populations for all types of crop residues emissions. The rBC-containing particles with lag-times < 2 μs were classified as uncoated or thinly-coated while those with lag-times > 2 μs were considered to have significant amounts of coatings and therefore classified as thickly-coated particles (Wang et al., 2016b). The degree of rBC mixing is expressed as the number fraction of thickly-coated rBC and calculated as the percentage of rBC-containing particles with lag-times > 2 μs.

2.3. Light absorption measurements

The light absorption coefficient (B_{abs}) of particles was directly measured with a Photoacoustic Extinctiometer (PAX, Droplet Measurement Technologies, Boulder, CO) at λ = 870 nm, which uses intracavity photoacoustic technology. A laser beam in the acoustic chamber of this instrument heats the sampled light-absorbing particles, and this heating produces a pressure wave that is detected with a sensitive microphone. Additionally, PAX also can simultaneously measure light scattering coefficient (B_{scat}) with a wide-angle integrating reciprocal nephelometer in the scattering chamber. Before the biomass-burning experiments, ammonium sulfate and freshly-generated propane BC were used to calibrate the B_{scat} and B_{abs}, respectively. The light extinction coefficient ($B_{ext} = B_{scat} + B_{abs}$) can be calculated from the laser power of the PAX; thus, a correction factor can be established from the relationship between the calculated B_{abs} ($= B_{ext} - B_{scat}$) and the measured B_{abs}. The equation of B_{ext} is given by:

$$B_{ext} = -\frac{1}{0.354} \times \ln\frac{I}{I_0} \times 10^6 \ [Mm^{-1}] \quad (1)$$

Table 1
Summary experiments of open burning of crop residues.

Crop residues	Crop producing province	Test number	Weight (g)	Dilution ratio	Combustion time (min)
Rice straw	Anhui, Hunan, Shandong, and Jiangxi	9	50.2–55.3	20–26	4–8
Wheat straw	Henan and Shaanxi	10	51.2–53.5	20–25	7–9
Corn stalk	Hebei, Henan, Hunan, Shandong, and Shaanxi	11	50.1–55.2	22–25	5–9
Cotton stalk	Anhui, Henan, Hunan, and Shandong	15	53.1–56.7	26–38	4–12
Soybean stalk	Anhui, Henan, Hunan, and Shaanxi	12	51.6–57.7	15–35	4–10

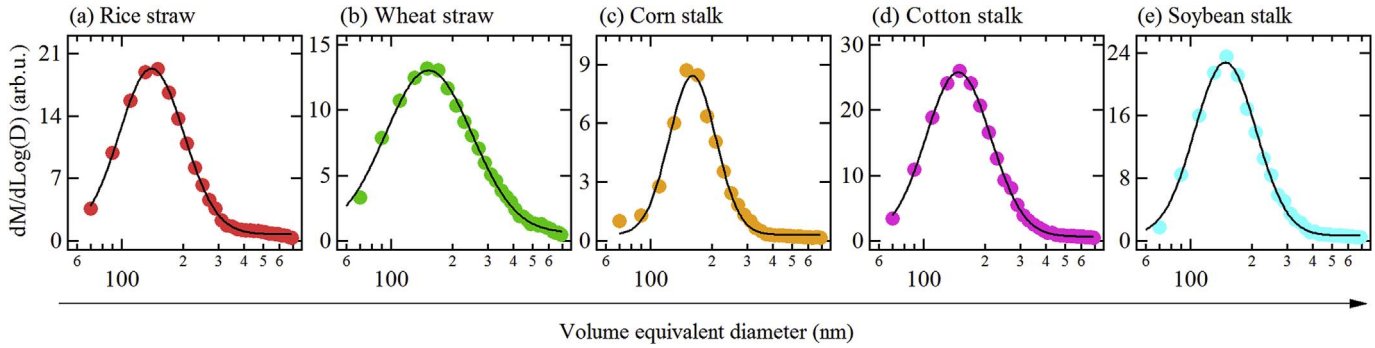

Fig. 2. Average mass size distributions of rBC in volume equivalent diameters for different crop residues emissions. The solid lines represent single mode lognormal fits.

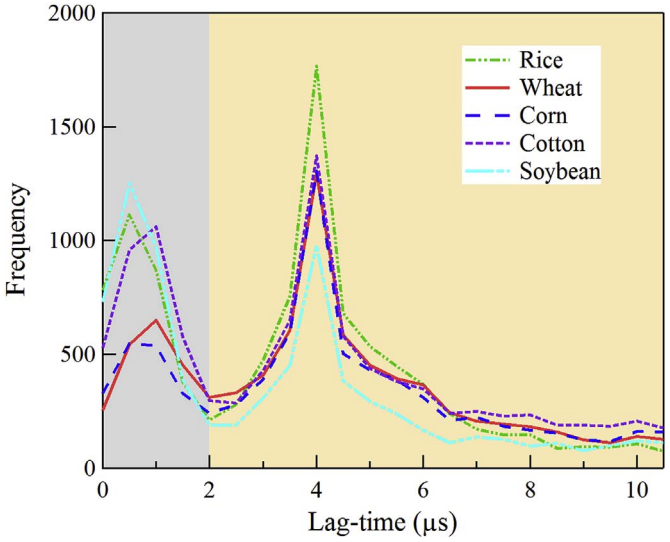

Fig. 3. Frequency distributions of the incandescence lag-times for ~1.1 × 10^4–1.5 × 10^4 arbitrary-selected rBC particles from different types of crop residues emissions. The light grey and light yellow regions represent the uncoated or thinly-coated rBC particles and the thickly-coated ones, respectively. (For interpretation of the references to colour in this figure legend, the reader is referred to the Web version of this article.)

where 0.354 is the path length of the laser beam through the cavity in meters; 10^6 is a conversion factor to express B_{ext} in Mm^{-1}; I_0 is the average laser power before and/or after calibration; and I is the laser power during calibration. Because the scattering produced by BC cannot be negligible, the B_{abs} is calculated by subtracting B_{scat} from B_{ext}. The B_{scat} should be calibrated first following the same calibration steps of B_{abs}. A linear relationship is then established between extinction-minus-scattering coefficient and measured B_{abs}. The slope of the linear regression is used as the correction factor inputted into the PAX as the new absorption factor. In this study, the same steps of absorption calibration were repeated until the correction factor was stable within ~5%.

2.4. Calculation of modified combustion efficiency (MCE)

The combustion conditions during each test burn were characterized by calculating the MCE, which is a function of the relative amounts of carbon emitted as CO_2 and carbon monoxide (CO) (Kondo et al., 2011):

$$MCE = \frac{\Delta[CO_2]}{\Delta[CO_2] + \Delta[CO]} \quad (2)$$

where $\Delta[CO_2]$ and $\Delta[CO]$ are the excess mixing ratios of CO_2 and CO, respectively, which are calculated by subtracting the combustion chamber background, that is, the air measured before ignition, from the values obtained during the test burn. Real-time CO_2 and CO mixing ratios were measured with a nondispersive infrared CO_2 analyzer (Model SBA-4, PP System, Amesbury, MA, USA) and a CO analyzer (Model 48i, Thermo Scientific Inc. Franklin, MA, USA), respectively.

3. Results and discussion

3.1. Size distributions of rBC cores

The mass-equivalent diameters of the rBC cores of the burning residues were well represented by mono-modal lognormal distributions (Fig. 2), and this finding is consistent with previous observations from both laboratory and field biomass-burning studies (Schwarz et al., 2008; May et al., 2014; Taylor et al., 2014). Fig. 4a shows the distributions of rBC mass median diameters (MMDs) of each test burn for the five types of crop residues emissions. The rBC MMDs were found in relatively narrow ranges, varying from 129–152, 136–159, 137–204, 133–157, and 132–163 nm for rice, wheat, corn, cotton, and soybean

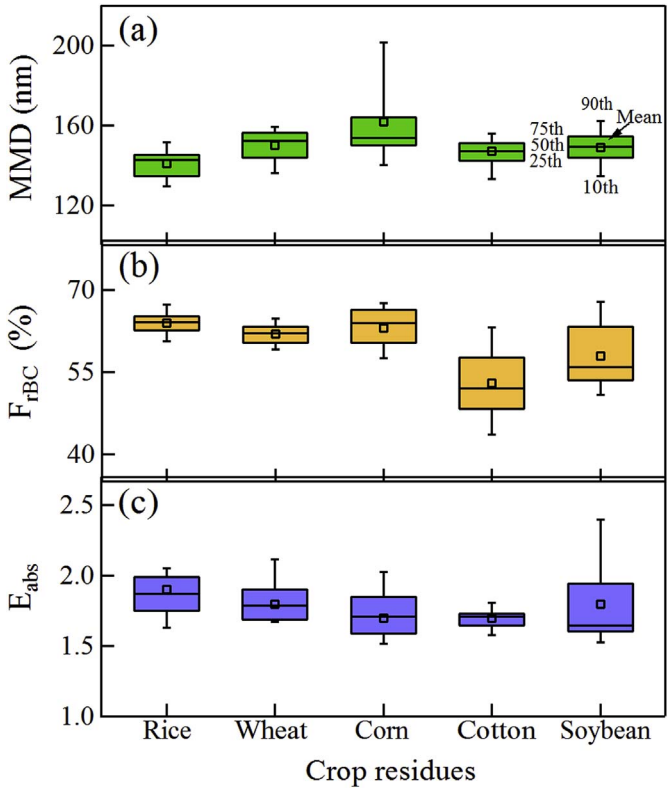

Fig. 4. Distributions of (a) rBC mass median diameter (MMD), (b) number fraction of thickly-coated rBC (F_{rBC}), and (c) light absorption enhancement (E_{abs}) for different types of crop residues emissions.

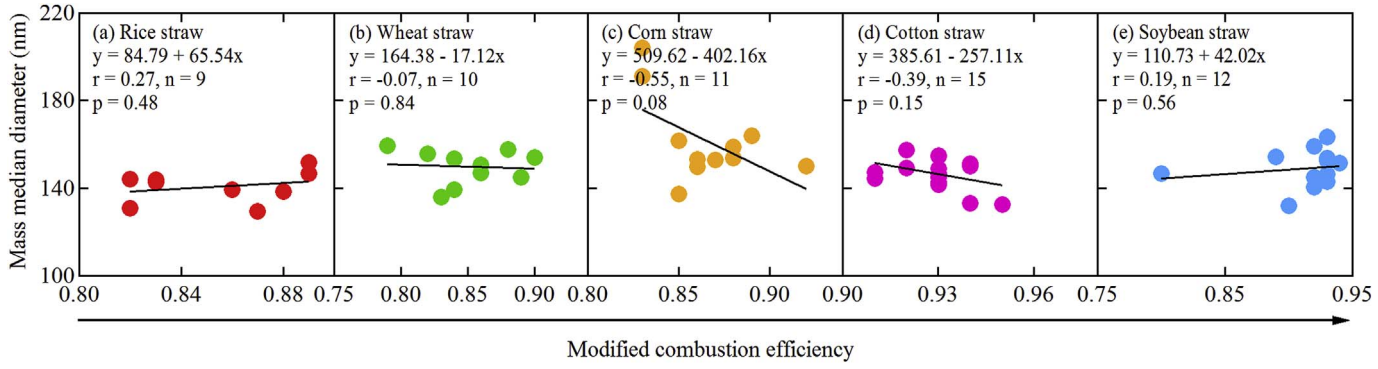
(a) Rice straw
y = 84.79 + 65.54x
r = 0.27, n = 9
p = 0.48
(b) Wheat straw
y = 164.38 - 17.12x
r = -0.07, n = 10
p = 0.84
(c) Corn straw
y = 509.62 - 402.16x
r = -0.55, n = 11
p = 0.08
(d) Cotton straw
y = 385.61 - 257.11x
r = -0.39, n = 15
p = 0.15
(e) Soybean straw
y = 110.73 + 42.02x
r = 0.19, n = 12
p = 0.56
Mass median diameter (nm)
Modified combustion efficiency

Fig. 5. Relationship between rBC mass median diameter and modified combustion efficiency for five types of crop residues emissions.

residues, respectively; with corresponding arithmetic mean values (± standard deviation, SD), also in nm, of 141 (± 7), 150 (± 8), 162 (± 19), 147 (± 7), and 149 (± 9). The student's *t*-tests for the rBC MMDs from the different types of fuels showed that there was a statistically significant difference at a probability for chance occurrence of < 5% (p = 0.002) between rice straw and corn stalk emissions while the differences for other types of crop residues emissions were not significant (p = 0.15 to 1.0).

The type of combustion, that is, whether the fire is flaming or smoldering, can lead to distinct differences in the properties of the emitted particles (Ni et al., 2015). The MCE values for the different test burns, which are a measure of how efficiently the fuels are burned (Yokelson et al., 1996), ranged from ~0.79 to 0.95, and this reflects the amount of variability in completeness of combustion from burn-to-burn. A MCE > 0.9 is characteristic of the flaming phase while a MCE < 0.9 represents the smoldering phase (Reid et al., 2005). Fig. 5 shows that the MMDs of the emissions correlated either weakly or insignificantly with the MCEs (r = −0.55 to 0.27 and p = 0.08 to 0.84), suggesting that the smoldering or flaming conditions had limited effects on the rBC core sizes. May et al. (2014) similarly found no clear relationship between MMDs and MCEs for the burning of some individual plant species in a laboratory combustion study. It should be noted that there were no test burns occurred under the condition of MCE > 0.95 in this study. Liu et al. (2014) reported that the single scattering albedo (scattering/(absorption + scattering)) from biomass burning dramatically decreased with the increasing MCE when it larger than 0.95, implying that large fraction of rBC may be produced. More rBC particles favor rBC-rBC coagulation, and thereby leads to increases in rBC core size. Thus, the bad correlation between MMDs and MCEs in this study may be also related to the relative weak rBC-rBC coagulation under MCE < 0.95.

Compared with previous biomass-burning observations made with an SP2, our average MMDs fall within the lower limits of ~140–190 nm from laboratory-based biomass-burning experiments reported by May et al. (2014). However, the average MMDs found in our study are considerably smaller than those for aircraft measurements (altitudes: ~1.8–5.0 km) made in biomass-burning plumes in the ambient atmosphere (Kondo et al., 2011; Sahu et al., 2012; Taylor et al., 2014). For example, Kondo et al. (2011) found that MMDs were 177–197 nm in fresh biomass-burning plumes (age < 1 day) that originated from North America and 176–238 nm in aged biomass-burning plumes (age: 2–3 days) from Asia. Taylor et al. (2014) reported MMDs of 194 nm (age: ~1 day) and 196 nm (age: ~2 days) in two biomass-burning plumes from a Canadian boreal forest. Sahu et al. (2012) observed MMDs of 172–210 nm for biomass-burning plumes encountered over different regions of California. In addition to the fact that different types of biomass (e.g., crop residues versus various forest vegetation) can produce distinct MMDs, the larger MMDs in ambient biomass-burning studies may be also related to their higher MCEs compared with our laboratory study. In most cases, only an active flaming fire (e.g., MCE > 0.95) can produce enough heat to convect the plume to higher altitudes, and the high MCE is favor to rBC-rBC coagulation leading to relative large MMDs. Moreover, another possible reason for the larger MMDs in the studies of the ambient atmosphere compared with our laboratory study is that atmospheric aging/coagulation processes may cause growth in rBC cores in the field as the particles in most of the ambient studies were sampled a day or more after their production.

3.2. Mixing state of rBC

Freshly emitted rBC particles are typically externally mixed with other aerosol components, but they become internally mixed through physicochemical aging processes in the atmosphere (China et al., 2015). In biomass-burning plumes, rBC particles are thought to become coated with other materials in the first few hours after emission (Akagi et al., 2012). A more efficient burning phase (flaming; MCE > 0.9) will favor production of rBC relative to organic aerosol, while less efficient burning condition (smoldering; MCE < 0.9) will tend to produce more organic aerosol compared with rBC, leading to large formation of thickly-coated rBC particles (Kondo et al., 2011; Collier et al., 2016). As shown in Fig. 4b, the average number fraction of thickly-coated rBC is comparable among different types of biomass-burning emissions, with arithmetic means ± SD (in %) of 64 ± 2, 62 ± 2, 63 ± 3, 53 ± 7, and 58 ± 6 for burning straw or stalks of rice, wheat, corn, cotton, and soybean, respectively; and this shows that the rBC particles were coated even though they were freshly emitted.

To investigate the potential influence of the MCE on rBC mixing state, the number fraction of thickly-coated rBC is plotted against MCEs in Fig. 6. Except for the emissions from rice straw burning, the thickly-coated rBC number fraction was found to be significantly anti-correlated (r = −0.73 to −0.65, p = 0.002 to 0.03) with the MCEs. This implies that when crop residues burn in smoldering fires, more coated rBC particles are produced compared with the particles produced by flaming fires. The larger implication of this finding is that differences in the types of both fuels and fires may affect the optical properties of the particles that are produced, and this in turn could influence their impact on radiative fluxes and hence climate.

3.3. Light absorption enhancement

The mass absorption cross-section (MAC, expressed in $m^2\ g^{-1}$) relates rBC mass concentrations to light absorption, and it is one of the key variables used in radiative transfer models (Bond et al., 2013). In our study, a MAC of rBC at λ = 870 nm (MAC_{870}) was calculated by dividing the absorption coefficient measured with the PAX by the rBC mass concentration detected with the SP2 (MAC_{870} = absorption/rBC). Fig. 7 shows that ~90% of the MAC_{870} values for all burning cases mainly fell within a relatively narrow range of 6.5–8.5 $m^2\ g^{-1}$, which are comparable with the values of 5.7–8.3 $m^2\ g^{-1}$ that are influenced by biomass-burning emissions in previous studies (Kondo et al., 2009;

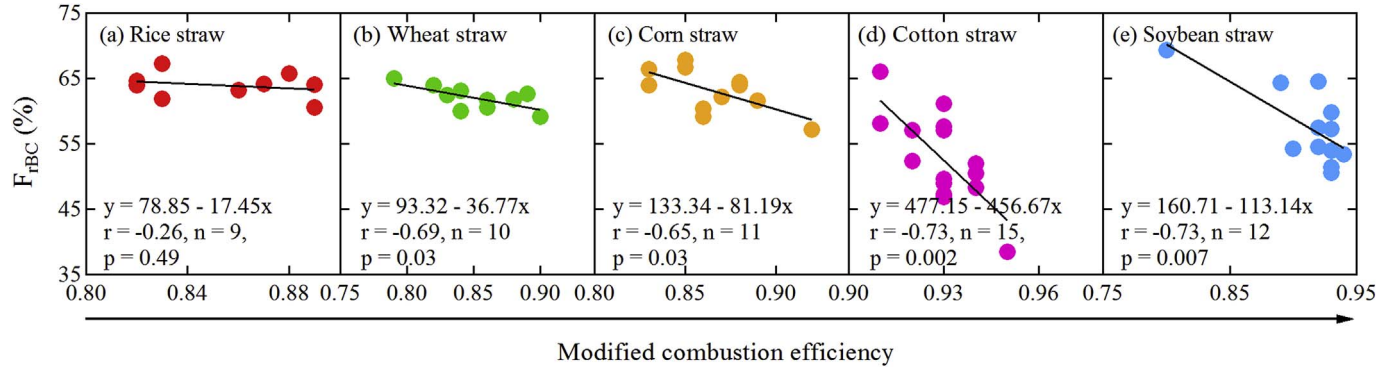
(a) Rice straw
(b) Wheat straw
(c) Corn straw
(d) Cotton straw
(e) Soybean straw
F_rBC (%)
y = 78.85 - 17.45x
r = -0.26, n = 9,
p = 0.49
y = 93.32 - 36.77x
r = -0.69, n = 10
p = 0.03
y = 133.34 - 81.19x
r = -0.65, n = 11
p = 0.03
y = 477.15 - 456.67x
r = -0.73, n = 15,
p = 0.002
y = 160.71 - 113.14x
r = -0.73, n = 12
p = 0.007
Modified combustion efficiency

Fig. 6. Relationship between number fraction of thickly-coated rBC (F_{rBC}) and modified combustion efficiency for five types of crop residues emissions.

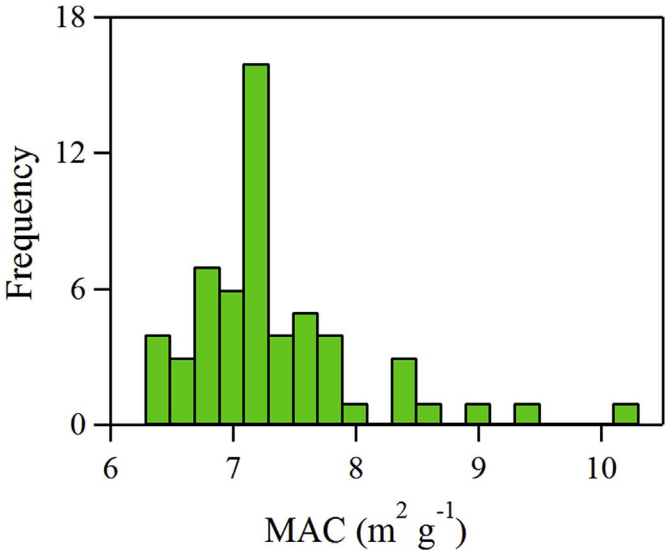

Fig. 7. Frequency distribution of rBC mass absorption cross section (MAC) for five types of crop residues emissions.

Subramanian et al., 2010; Laborde et al., 2013; Wang et al., 2015). Average MAC_{870} (± SD) for the rBC particles from rice, wheat, corn, cotton, and soybean burning were 7.6 ± 0.5, 7.5 ± 0.6, 7.2 ± 0.6, 7.0 ± 0.3, and 7.4 ± 1.3 $m^2 g^{-1}$, respectively. The *t*-tests showed that the differences in MAC_{870} among the various crop types were not statistically significant at a probability of 5% (p = 0.06), suggesting that the absorption capacity of the rBC normalized by mass was independent on the type of plant matter burned.

Based on the assumption of spherical for uncoated rBC particles, Mie theory was used to calculate the MAC_{870} of uncoated rBC particles ($MAC_{870,uncoated}$) using the core sizes of rBC measured with the SP2. More details regarding the Mie algorithms can be found in Bohren and Huffman (2008). For uncoated rBC, we used a refractive index of 1.85–0.71*i* at λ = 550 nm, which is in the middle of the range suggested by Bond and Bergstrom (2006). Mie theory was first applied to estimate the MAC values of uncoated rBC at λ = 550 nm, and then those values were converted to $MAC_{870,uncoated}$ based on an rBC absorption Ångström exponent of 1.0 (Lack and Langridge, 2013). The average absorption enhancement was calculated by comparing MAC_{870} for rBC with and without coatings (Enhancement = $MAC_{870}/MAC_{870,uncoated}$).

Large absorption enhancements were found in the fresh biomass-burning emissions, with average values of 1.9 ± 0.1, 1.8 ± 0.1, 1.7 ± 0.2, 1.7 ± 0.1, and 1.8 ± 0.3 for straw or stalks of rice, wheat, corn, cotton, and soybean emissions, respectively (Fig. 4c). These observations suggest that light absorption for relatively fresh rBC is enhanced compared with that for uncoated particles. The refractive index of rBC is a key input parameter in the Mie model, and we bounded our calculations using the lowest (1.75–0.63*i*) and highest (1.95–0.79*i*) refractive index values suggested by Bond and Bergstrom (2006). This was done to evaluate the sensitivity of absorption enhancement calculations to the parameterization of the refractive index, and the results show that the difference between the two extreme cases was within ~15%.

To further investigate the potential impacts of rBC morphology and mixing state on light absorption, we plotted the absorption enhancement values against the number fraction of thickly-coated rBC and against the MMDs. As shown in Fig. 8(a–e), except for the rice straw case, absorption enhancement was positively correlated (r = 0.72 to 0.79, and p = 0.003 to 0.009) with the number fraction of thickly-coated rBC, suggesting that the magnitude of the light absorption enhancement was strongly affected by the amounts of coatings on the particles. There is a good explanation for this; that is, light absorption caused by coated rBC is "enhanced" because the coatings act as a lens that refracts more light to the particle's core, which is called "lensing effects" (Lack and Cappa, 2010). Previous studies have shown that even if for the same amount of coatings, BC embedded within a particle of non-BC compounds can cause larger enhancement for MAC than the one attached to the surface of a non-BC particle (Fuller et al., 1999; Scarnato et al., 2013). The poor correlation for rice straw emissions here may be due to the different internal morphology of rBC compared with other crop residues emissions. However, this speculation needs further evidence in the future work. In addition to the coating amount, the rBC core size may also affect the absorption enhancement, because it provides a surface area to receive the incident light. Fig. 8(f–j) shows that there was no clear relationship between absorption enhancement and MMDs, suggesting that the absorption enhancement of coated rBC particles is independent of the rBC core size at the range of ~129–204 nm. Thus, light absorption enhancement of rBC-containing particles is apparently affected by the "lensing effects" of the coatings.

4. Conclusions and atmospheric implications

We investigated the physicochemical properties of rBC particles produced in laboratory studies of open biomass burning, and one main focus of this work was on the optical properties of the particles and how they were affected by coatings on the particles. Our results showed that average rBC core size ranged from 141 to 162 nm for different types of crop residues emissions regardless of whether the fires were in the smoldering or flaming phase. Large number fractions of thickly-coated rBC (53–64%) were found in the freshly emitted particles. Smoldering crop residues tended to produce more coated rBC than flaming fires. The average rBC MAC_{870} for different kinds of crop residues varied from 7.0 to 7.6 $m^2 g^{-1}$. The *t*-tests showed that light absorption capacity of the rBC particles was independent of the types of crop residues that were burned. By comparing the result of observed MAC_{870} with SP2 and PAX to that calculated with the Mie theory, it indicated that freshly

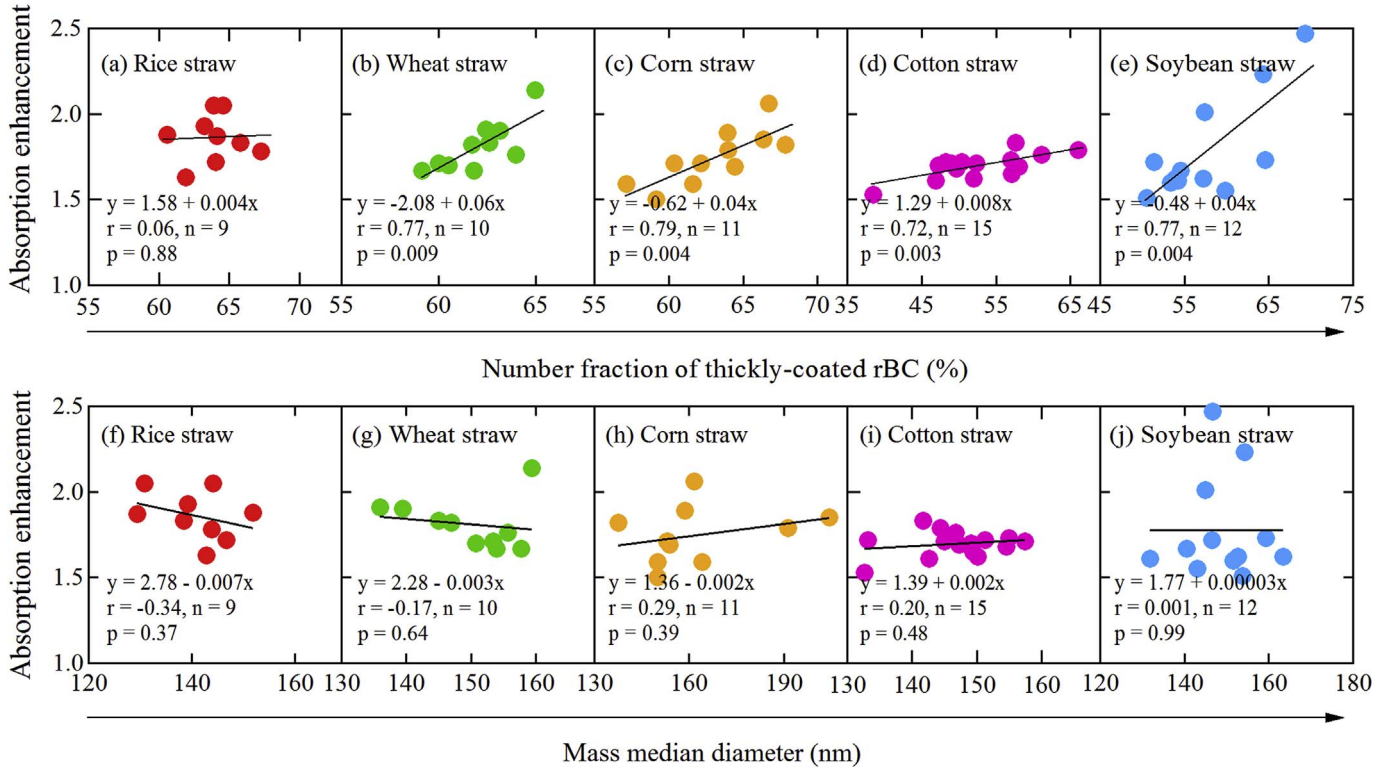
(a) Rice straw
y = 1.58 + 0.004x
r = 0.06, n = 9
p = 0.88
(b) Wheat straw
y = -2.08 + 0.06x
r = 0.77, n = 10
p = 0.009
(c) Corn straw
y = -0.62 + 0.04x
r = 0.79, n = 11
p = 0.004
(d) Cotton straw
y = 1.29 + 0.008x
r = 0.72, n = 15
p = 0.003
(e) Soybean straw
y = -0.48 + 0.04x
r = 0.77, n = 12
p = 0.004
Absorption enhancement
Number fraction of thickly-coated rBC (%)
(f) Rice straw
y = 2.78 - 0.007x
r = -0.34, n = 9
p = 0.37
(g) Wheat straw
y = 2.28 - 0.003x
r = -0.17, n = 10
p = 0.64
(h) Corn straw
y = 1.36 - 0.002x
r = 0.29, n = 11
p = 0.39
(i) Cotton straw
y = 1.39 + 0.002x
r = 0.20, n = 15
p = 0.48
(j) Soybean straw
y = 1.77 + 0.00003x
r = 0.001, n = 12
p = 0.99
Absorption enhancement
Mass median diameter (nm)

Fig. 8. Scatterplot of absorption enhancement versus (a–e) number fraction of thickly-coated rBC and (f–j) rBC mass median diameter for different types of crop residues emissions. The solid line fits were calculated by orthogonal regression.

emitted biomass-burning rBC particles had large light absorption enhancements compared with uncoated particles, with values of 1.7–1.9. The absorption enhancements were positively correlation with the number fraction of thickly-coated rBC, but there was no clear relationship with the rBC core size. This implies that absorption enhancement of internally-mixed rBC is the result of "lensing effects" caused by the coatings.

For this study, there are at least three key implications for our findings (1) the open burning of crop residues may cause strong positive direct radiative forcing immediately after their production because a large fraction of the freshly emitted rBC particles have substantial coatings that cause increased light absorption; (2) the enhanced optical properties of rBC could contribute in significant ways to stabilization atmosphere through heating in the planetary boundary layer and in so doing depress the development of the planetary boundary layer which could increase the likelihood and severity of haze events; and (3) the presence of coatings and large absorption enhancement in rBC from fresh biomass-burning emissions implies that atmospheric aging may have limited effects on rBC light absorption although changes in the chemical composition of coatings with time could still affect how the particles interact with light. Each of these topics will be important for further research on the effects of biomass-burning emissions on the Earth's radiative balance and climate.

Acknowledgments

This study was supported by the National Natural Science Foundation of China (41230641, 41503118, 41661144020, and 41625015) and China Postdoctoral Science Foundation (2015M580890).

References

Akagi, S.K., Craven, J.S., Taylor, J.W., McMeeking, G.R., Yokelson, R.J., Burling, I.R., Urbanski, S.P., Wold, C.E., Seinfeld, J.H., Coe, H., Alvarado, M.J., Weise, D.R., 2012. Evolution of trace gases and particles emitted by a chaparral fire in California. Atmos. Chem. Phys. 12, 1397–1421. https://doi.org/10.5194/acp-12-1397-2012.

Bauer, S.E., Menon, S., Koch, D., Bond, T.C., Tsigaridis, K., 2010. A global modeling study on carbonaceous aerosol microphysical characteristics and radiative effects. Atmos. Chem. Phys. 10, 7439–7456. https://doi.org/10.5194/acp-10-7439-2010.

Bohren, C.F., Huffman, D.R., 2008. Absorption and Scattering of Light by Small Particles. John Wiley & Sons, New York.

Bond, T.C., Bergstrom, R.W., 2006. Light absorption by carbonaceous particles: an investigative review. Aerosol. Sci. Technol. 40, 27–67. https://doi.org/10.1080/02786820500421521.

Bond, T.C., Doherty, S.J., Fahey, D.W., Forster, P.M., Berntsen, T., DeAngelo, B.J., Flanner, M.G., Ghan, S., Karcher, B., Koch, D., Kinne, S., Kondo, Y., Quinn, P.K., Sarofim, M.C., Schultz, M.G., Schulz, M., Venkataraman, C., Zhang, H., Zhang, S., Bellouin, N., Guttikunda, S.K., Hopke, P.K., Jacobson, M.Z., Kaiser, J.W., Klimont, Z., Lohmann, U., Schwarz, J.P., Shindell, D., Storelvmo, T., Warren, S.G., Zender, C.S., 2013. Bounding the role of black carbon in the climate system: a scientific assessment. J. Geophys. Res. Atmos. 118, 5380–5552. http://dx.doi.org/10.1002/jgrd.50171.

Booth, B., Bellouin, N., 2015. Climate change: black carbon and atmospheric feedbacks. Nature 519, 167–168. http://dx.doi.org/10.1038/519167a.

Cappa, C.D., Onasch, T.B., Massoli, P., Worsnop, D.R., Bates, T.S., Cross, E.S., Davidovits, P., Hakala, J., Hayden, K.L., Jobson, B.T., Kolesar, K.R., Lack, D.A., Lerner, B.M., Li, S.-M., Mellon, D., Nuaaman, I., Olfert, J.S., Petaja, T., Quinn, P.K., Song, C., Subramanian, R., Williams, E.J., Zaveri, R.A., 2012. Radiative absorption enhancements due to the mixing state of atmospheric black carbon. Science 337, 1078–1081. http://dx.doi.org/10.1126/science.1223447.

Chen, J., Li, C., Ristovski, Z., Milic, A., Gu, Y., Islam, M.S., Wang, S., Hao, J., Zhang, H., He, C., Guo, H., Fu, H., Miljevic, B., Morawska, L., Phong, T., Fat, Y.L.A.M., Pereira, G., Ding, A., Huang, X., Dumka, U.C., 2017. A review of biomass burning: emissions and impacts on air quality, health and climate in China. Sci. Total Environ. 579, 1000–1034. https://doi.org/10.1016/j.scitotenv.2016.11.025.

China, S., Scarnato, B., Owen, R.C., Zhang, B., Ampadu, M.T., Kumar, S., Dzepina, K., Dziobak, M.P., Fialho, P., Perlinger, J.A., Hueber, J., Helmig, D., Mazzoleni, L.R., Mazzoleni, C., 2015. Morphology and mixing state of aged soot particles at a remote marine free troposphere site: implications for optical properties. Geophys. Res. Lett. 42, 1243–1250. http://dx.doi.org/10.1002/2014GL062404.

China Statistical Yearbook, 2016, http://www.stats.gov.cn/tjsj/ndsj/2016/indexch.htm.

Collier, S., Zhou, S., Onasch, T.B., Jaffe, D.A., Kleinman, L., Sedlacek, A.J., Briggs, N.L., Hee, J., Fortner, E., Shilling, J.E., Worsnop, D., Yokelson, R.J., Parworth, C., Ge, X.L., Xu, J.Z., Butterfield, Z., Chand, D., Dubey, M.K., Pekour, M.S., Springston, S., Zhang, Q., 2016. Regional influence of aerosol emissions from wildfires driven by combustion efficiency: insights from the BBOP campaign. Environ. Sci. Technol. 50, 8613–8622. http://dx.doi.org/10.1021/acs.est.6b01617.

Ding, A.J., Huang, X., Nie, W., Sun, J.N., Kerminen, V.M., Petaja, T., Su, H., Cheng, Y.F., Yang, X.Q., Wang, M.H., Chi, X.G., Wang, J.P., Virkkula, A., Guo, W.D., Yuan, J.,

Wang, S.Y., Zhang, R.J., Wu, Y.F., Song, Y., Zhu, T., Zilitinkevich, S., Kulmala, M., Fu, C.B., 2016. Enhanced haze pollution by black carbon in megacities in China. Geophys. Res. Lett. 43, 2873–2879. http://dx.doi.org/10.1002/2016GL067745.

Forbes, M.S., Raison, R.J., Skjemstad, J.O., 2006. Formation, transformation and transport of black carbon (charcoal) in terrestrial and aquatic ecosystems. Sci. Total Environ. 370, 190–206. https://doi.org/10.1016/j.scitotenv.2006.06.007.

Fuller, K.A., Malm, W.C., Kreidenweis, S.M., 1999. Effects of mixing on extinction by carbonaceous particles. J. Geophys. Res. 104, 15941–15954. http://dx.doi.org/10.1029/1998JD100069.

Gao, R.S., Schwarz, J.P., Kelly, K.K., Fahey, D.W., Watts, L.A., Thompson, T.L., Spackman, J.R., Slowik, J.G., Cross, E.S., Han, J.H., Davidovits, P., Onasch, T.B., Worsnop, D.R., 2007. A novel method for estimating light-scattering properties of soot aerosols using a modified single-particle soot photometer. Aerosol. Sci. Technol. 41, 125–135. https://doi.org/10.1080/02786820601118398.

Hodnebrog, O., Myhre, G., Forster, P.M., Sillmann, J., Samset, B.H., 2016. Local biomass burning is a dominant cause of the observed precipitation reduction in southern Africa. Nat. Commun. 7. http://dx.doi.org/10.1038/ncomms11236.

Jacobson, M.Z., 2001. Strong radiative heating due to the mixing state of black carbon in atmospheric aerosols. Nature 409, 695–697. http://dx.doi.org/10.1038/35055518.

Kondo, Y., Sahu, L., Kuwata, M., Miyazaki, Y., Takegawa, N., Moteki, N., Imaru, J., Han, S., Nakayama, T., Oanh, N.T.K., Hu, M., Kim, Y.J., Kita, K., 2009. Stabilization of the mass absorption cross section of black carbon for filter-based absorption photometry by the use of a heated inlet. Aerosol. Sci. Technol. 43, 741–756. https://doi.org/10.1080/02786820902889879.

Kondo, Y., Matsui, H., Moteki, N., Sahu, L., Takegawa, N., Kajino, M., Zhao, Y., Cubison, M.J., Jimenez, J.L., Vay, S., Diskin, G.S., Anderson, B., Wisthaler, A., Mikoviny, T., Fuelberg, H.E., Blake, D.R., Huey, G., Weinheimer, A.J., Knapp, D.J., Brune, W.H., 2011. Emissions of black carbon, organic, and inorganic aerosols from biomass burning in North America and Asia in 2008. J. Geophys. Res. Atmos. 116, D08204. http://dx.doi.org/10.1029/2010JD015152.

Laborde, M., Crippa, M., Tritscher, T., Jurányi, Z., Decarlo, P.F., Temime-Roussel, B., Marchand, N., Eckhardt, S., Stohl, A., Baltensperger, U., Prévôt, A.S.H., Weingartner, E., Gysel, M., 2013. Black carbon physical properties and mixing state in the European megacity Paris. Atmos. Chem. Phys. 13, 5831–5856. https://doi.org/10.5194/acp-13-5831-2013.

Lack, D.A., Cappa, C.D., 2010. Impact of brown and clear carbon on light absorption enhancement, single scatter albedo and absorption wavelength dependence of black carbon. Atmos. Chem. Phys. 10, 4207–4220. https://doi.org/10.5194/acp-10-4207-2010.

Lack, D.A., Langridge, J.M., 2013. On the attribution of black and brown carbon light absorption using the Angstrom exponent. Atmos. Chem. Phys. 13, 10535–10543. https://doi.org/10.5194/acp-13-10535-2013.

Lan, Z.-J., Huang, X.-F., Yu, K.-Y., Sun, T.-L., Zeng, L.-W., Hu, M., 2013. Light absorption of black carbon aerosol and its enhancement by mixing state in an urban atmosphere in South China. Atmos. Environ. 69, 118–123. https://doi.org/10.1016/j.atmosenv.2012.12.009.

Li, Y., Henze, D.K., Jack, D., Henderson, B.H., Kinney, P.L., 2016. Assessing public health burden associated with exposure to ambient black carbon in the United States. Sci. Total Environ. 539, 515–525. https://doi.org/10.1016/j.scitotenv.2015.08.129.

Liu, S., Aiken, A.C., Arata, C., Dubey, M.K., Stockwell, C.E., Yokelson, R.J., Stone, E.A., Jayarathne, T., Robinson, A.L., DeMott, P.J., Kreidenweis, S.M., 2014. Aerosol single scattering albedo dependence on biomass combustion efficiency: laboratory and field studies. Geophys. Res. Lett. 41 (2), 742–748. http://dx.doi.org/10.1002/2013GL058392.

Liu, S., Aiken, A.C., Gorkowski, K., Dubey, M.K., Cappa, C.D., Williams, L.R., Herndon, S.C., Massoli, P., Fortner, E.C., Chhabra, P.S., Brooks, W.A., Onasch, T.B., Jayne, J.T., Worsnop, D.R., China, S., Sharma, N., Mazzoleni, C., Xu, L., Ng, N.L., Liu, D., Allan, J.D., Lee, J.D., Fleming, Z.L., Mohr, C., Zotter, P., Szidat, S., Prevot, A.S.H., 2015. Enhanced light absorption by mixed source black and brown carbon particles in UK winter. Nat. Commun. 6. http://dx.doi.org/10.1038/ncomms9435.

Long, X., Tie, X., Cao, J., Huang, R., Feng, T., Li, N., Zhao, S., Tian, J., Li, G., Zhang, Q., 2016. Impact of crop field burning and mountains on heavy haze in the North China Plain: a case study. Atmos. Chem. Phys. 16, 9675–9691. https://doi.org/10.5194/acp-16-9675-2016.

May, A.A., McMeeking, G.R., Lee, T., Taylor, J.W., Craven, J.S., Burling, I., Sullivan, A.P., Akagi, S., Collett Jr., J.L., Flynn, M., Coe, H., Urbanski, S.P., Seinfeld, J.H., Yokelson, R.J., Kreidenweis, S.M., 2014. Aerosol emissions from prescribed fires in the United States: a synthesis of laboratory and aircraft measurements. J. Geophys. Res. Atmos. 119, 11826–11849. http://dx.doi.org/10.1002/2014JD021848.

Ni, H., Han, Y., Cao, J., Chen, L.W.A., Tian, J., Wang, X., Chow, J.C., Watson, J.G., Wang, Q., Wang, P., Li, H., Huang, R.-J., 2015. Emission characteristics of carbonaceous particles and trace gases from open burning of crop residues in China. Atmos. Environ. 123, 399–406. https://doi.org/10.1016/j.atmosenv.2015.05.007.

Peng, J., Hu, M., Guo, S., Du, Z., Zheng, J., Shang, D., Zamora, M.L., Zeng, L., Shao, M., Wu, Y.-S., Zheng, J., Wang, Y., Glen, C.R., Collins, D.R., Molina, M.J., Zhang, R., 2016. Markedly enhanced absorption and direct radiative forcing of black carbon under polluted urban environments. Proc. Natl. Acad. Sci. U. S. A. 113, 4266–4271. https://doi.org/10.1073/pnas.1602310113.

Qiu, X., Duan, L., Chai, F., Wang, S., Yu, Q., Wang, S., 2016. Deriving high-resolution emission inventory of open biomass burning in China based on satellite observations. Environ. Sci. Technol. 50, 11779–11786. http://dx.doi.org/10.1021/acs.est.6b02705.

Ramanathan, V., Carmichael, G., 2008. Global and regional climate changes due to black carbon. Nat. Geosci. 1, 221–227. http://dx.doi.org/10.1038/ngeo156.

Reid, J.S., Koppmann, R., Eck, T.F., Eleuterio, D.P., 2005. A review of biomass burning emissions part II: intensive physical properties of biomass burning particles. Atmos. Chem. Phys. 5, 799–825. https://doi.org/10.5194/acp-5-799-2005.

Sahu, L.K., Kondo, Y., Moteki, N., Takegawa, N., Zhao, Y., Cubison, M.J., Jimenez, J.L., Vay, S., Diskin, G.S., Wisthaler, A., Mikoviny, T., Huey, L.G., Weinheimer, A.J., Knapp, D.J., 2012. Emission characteristics of black carbon in anthropogenic and biomass burning plumes over California during ARCTAS-CARB 2008. J. Geophys. Res. Atmos. 117, D16302. http://dx.doi.org/10.1029/2011JD017401.

Scarnato, B.V., Vahidinia, S., Richard, D.T., Kirchstetter, T.W., 2013. Effects of internal mixing and aggregate morphology on optical properties of black carbon using a discrete dipole approximation model. Atmos. Chem. Phys. 13, 5089–5101. https://doi.org/10.5194/acp-13-5089-2013.

Schwarz, J.P., Gao, R.S., Fahey, D.W., Thomson, D.S., Watts, L.A., Wilson, J.C., Reeves, J.M., Darbeheshti, M., Baumgardner, D.G., Kok, G.L., Chung, S.H., Schulz, M., Hendricks, J., Lauer, A., Kaercher, B., Slowik, J.G., Rosenlof, K.H., Thompson, T.L., Langford, A.O., Loewenstein, M., Aikin, K.C., 2006. Single-particle measurements of midlatitude black carbon and light-scattering aerosols from the boundary layer to the lower stratosphere. J. Geophys. Res. Atmos. 111, D16207. http://dx.doi.org/10.1029/2006jd007076.

Schwarz, J.P., Gao, R.S., Spackman, J.R., Watts, L.A., Thomson, D.S., Fahey, D.W., Ryerson, T.B., Peischl, J., Holloway, J.S., Trainer, M., Frost, G.J., Baynard, T., Lack, D.A., de Gouw, J.A., Warneke, C., Del Negro, L.A., 2008. Measurement of the mixing state, mass, and optical size of individual black carbon particles in urban and biomass burning emissions. Geophys. Res. Lett. 35 (13), L13810. http://dx.doi.org/10.1029/2008gl033968.

Slowik, J.G., Cross, E.S., Han, J.-H., Davidovits, P., Onasch, T.B., Jayne, J.T., WilliamS, L.R., Canagaratna, M.R., Worsnop, D.R., Chakrabarty, R.K., Moosmueller, H., Arnott, W.P., Schwarz, J.P., Gao, R.-S., Fahey, D.W., Kok, G.L., Petzold, A., 2007. An intercomparison of instruments measuring black carbon content of soot particles. Aerosol. Sci. Technol. 41, 295–314. https://doi.org/10.1080/02786820701197078.

Subramanian, R., Kok, G.L., Baumgardner, D., Clarke, A., Shinozuka, Y., Campos, T.L., Heizer, C.G., Stephens, B.B., de Foy, B., Voss, P.B., Zaveri, R.A., 2010. Black carbon over Mexico: the effect of atmospheric transport on mixing state, mass absorption cross-section, and BC/CO ratios. Atmos. Chem. Phys. 10, 219–237. https://doi.org/10.5194/acp-10-219-2010.

Taylor, J.W., Allan, J.D., Allen, G., Coe, H., Williams, P.I., Flynn, M.J., Le Breton, M., Muller, J.B.A., Percival, C.J., Oram, D., Forster, G., Lee, J.D., Rickard, A.R., Parrington, M., Palmer, P.I., 2014. Size-dependent wet removal of black carbon in Canadian biomass burning plumes. Atmos. Chem. Phys. 14, 13755–13771. https://doi.org/10.5194/acp-14-13755-2014.

Tian, J., Chow, J.C., Cao, J., Han, Y., Ni, H., Chen, L.W.A., Wang, X., Huang, R., Moosmueller, H., Watson, J.G., 2015. A biomass combustion chamber: design, evaluation, and a case study of wheat straw combustion emission tests. Aerosol Air Qual. Res. 15, 2104–2114. http://dx.doi.org/10.4209/aaqr.2015.03.0167.

Tollefsen, P., Rypdal, K., Torvanger, A., Rive, N., 2009. Air pollution policies in Europe: efficiency gains from integrating climate effects with damage costs to health and crops. Environ. Sci. Pol. 12, 870–881. https://doi.org/10.1016/j.envsci.2009.08.006.

Wang, Q., Huang, R.-J., Zhao, Z., Cao, J., Ni, H., Tie, X., Zhao, S., Su, X., Han, Y., Shen, Z., Wang, Y., Zhang, N., Zhou, Y., Corbin, J.C., 2016a. Physicochemical characteristics of black carbon aerosol and its radiative impact in a polluted urban area of China. J. Geophys. Res. Atmos. 121, 12505–12519. http://dx.doi.org/10.1002/2016JD024748.

Wang, Q., Huang, R.-J., Zhao, Z., Zhang, N., Wang, Y., Ni, H., Tie, X., Han, Y., Zhuang, M., Wang, M., Zhang, J., Zhang, X., Dusek, U., Cao, J., 2016b. Size distribution and mixing state of refractory black carbon aerosol from a coastal city in South China. Atmos. Res. 181, 163–171. https://doi.org/10.1016/j.atmosres.2016.06.022.

Wang, Q., Huang, R.J., Cao, J., Han, Y., Wang, G., Li, G., Wang, Y., Dai, W., Zhang, R., Zhou, Y., 2014a. Mixing state of black carbon aerosol in a heavily polluted urban area of China: implications for light absorption enhancement. Aerosol. Sci. Technol. 48, 689–697. https://doi.org/10.1080/02786826.2014.917758.

Wang, Q., Schwarz, J.P., Cao, J., Gao, R., Fahey, D.W., Hu, T., Huang, R.J., Han, Y., Shen, Z., 2014b. Black carbon aerosol characterization in a remote area of Qinghai-Tibetan Plateau, western China. Sci. Total Environ. 479, 151–158. https://doi.org/10.1016/j.scitotenv.2014.01.098.

Wang, Q.Y., Huang, R.J., Cao, J.J., Tie, X.X., Ni, H.Y., Zhou, Y.Q., Han, Y.M., Hu, T.F., Zhu, C.S., Feng, T., Li, N., Li, J.D., 2015. Black carbon aerosol in winter northeastern Qinghai–Tibetan Plateau, China: the source, mixing state and optical property. Atmos. Chem. Phys. 15, 13059–13069. https://doi.org/10.5194/acp-15-13059-2015.

Yokelson, R.J., Griffith, D.W.T., Ward, D.E., 1996. Open-path Fourier transform infrared studies of large-scale laboratory biomass fires. J. Geophys. Res. Atmos. 101, 21067–21080. http://dx.doi.org/10.1029/96JD01800.

Zha, S., Zhang, S., Cheng, T., Chen, J., Huang, G., Li, X., Wang, Q., 2013. Agricultural fires and their potential impacts on regional air quality over China. Aerosol Air Qual. Res. 13, 992–1001. http://dx.doi.org/10.4209/aaqr.2012.10.0277.